

HYBRID ENERGY MANAGEMENT-BASED INTELLIGENT ANFIS CONTROL FOR SMART DC-MICROGRID

DHARMASOTH YASHASWINI¹, I.VIJAY KUMAR², M. SRIKAR³, DR.T. ANIL KUMAR⁴

¹PG Scholar, Department of Electrical and Electronics Engineering, Anurag Group of Institutions (Anurag University), Venkatapur, Ghatkesar, Medchal Malkajgiri District, Telangana, India 500088

^{2,3}Assistant Professor, Department of Electrical and Electronics Engineering, Anurag University, Venkatapur, Ghatkesar, Medchal Malkajgiri District, Telangana, India 500088

⁴Professor, Department of Electrical and Electronics Engineering, Anurag University, Venkatapur, Ghatkesar, Medchal Malkajgiri District, Telangana, India 500088

Abstract: Adaptive Neuro Fuzzy Inference System (ANFIS) controller approach for a smart DC-microgrid is the primary goal of this work. In this project, a DC-microgrid is created by combining photovoltaic (PV), wind (WE), and a battery bank. Wind and solar power can be extracted at their optimum efficiency and power quality can be improved by a novel intelligent FOPID control technique for the source-side converter (SSCs) and the load side converter controlled by proposed ANFIS control technique. Prioritizing (PV and wind) energy sources helps the microgrid to be as cost effective as possible. The recommended ANFIS controller is designed to provide stable and smooth output power. Results from Matlab/Simulink simulations of the proposed control method are shown and compared to the existing mutual fuzzy logic and FO-PID controller.

Key words: Photovoltaic (PV), Wind Energy (WE), Battery, Adaptive Neuro Fuzzy Inference System (ANFIS), DC-microgrid,

I. INTRODUCTION

During the generation of electricity, a broad range of contaminants are released into the environment. For the most part, air pollution derives from thermal power plants since they burn fossil fuels (oil and coal). Nuclear power plant construction accelerated during the oil crisis had no discernible influence on air quality surrounding it. Therefore, radioactive waste is produced, causing substantial logistical issues. Because of the openness of the electrical market and the fear of relying only on one energy source, renewable energies have become more significant than ever in the production of power. [1] There are phasing issues as a result of the uneven distribution of energy use across end users. When the quantity of energy generated and consumed is equal, the grid is stable. Energy storage devices may be used in many different ways to make renewable energy a more viable option for the energy business. Energy storage is important in order to make this power more broadly accessible. As a result of this new technology, grid operators will be able to utilize the maximum amount of renewable energy feasible without resorting to load shedding when the output increases. In order to increase energy network resilience, islanding the supply region would enable local renewable production and local storage. [5–6] It is possible to increase the quality of the electricity delivered even during times of high demand by using an energy storage system with better control over frequency and voltage. A new research is looking at how a standalone microgrid might include renewable energy sources and energy storage. The maximum capacity of an energy storage system may be increased by combining tidal, wind, and PV energy sources. A battery and a supercapacitor are common components of energy storage systems (ESS), allowing the battery to last longer while also offering a rapid reaction to compensate for transient occurrences. As a result, the AC grid is used instead of supercapacitors when all energy sources are combined. Both DC and AC micro grids may be used in the same system. As a result, DC microgrids have a number of benefits over AC microgrids when it

comes to their integration and building simplicity. A different set of considerations is required when designing an AC system. These include information on things like frequency synchronization and reactive power. Similarly to an AC micro grid, a DC micro grid may be implemented in a number of ways, either as a standalone system or as part of an overall system. Self-sufficient DC microgrids may now run at their maximum efficiency thanks to recent advances in power electronics. Unpredictability makes it imperative to manage renewable energy supplies properly. The dynamic disparities between AC and DC microgrids have generated several research on AC microgrid energy management control. These techniques of control are not compatible with DC microgrids. A conventional DC microgrid is used to connect the load converters and energy sources for the DC-link. The DC-link voltage must be controlled for a stable and efficient DC microgrid [11, 12]. In the literature, the DC-link voltage has been the focus of several control approaches. [13] discusses energy resource planning and management in conjunction with hybrid micro grids. According to [14], fuzzy controllers and voltage management may be used to adjust DC voltage. A fuzzy logic control method based on reduced rule fuzzy logic is investigated in [15]. Dual proportional-integral controllers should be used. Only linear and time-limited methods are available for dealing with the DC-link. Research on several types of energy storage technologies for microgrids has been extensive. In the H control method is quite successful. Backstepping control is discussed in [16]. Lyapunov-based control and feedback linearization are examined in [17]. The paper [18] investigates the hybrid controller by combining backstepping and sliding mode controllers. This has led to this conclusion. Most of these controllers are vulnerable to fixed profits due to external shocks and parameter uncertainty. To wrap things off, we'll talk about how to regulate your own energy. For hybrid energy management, a new fractional order PID controller is developed using fuzzy logic to address issues with classic integer controllers. It is advantageous to use fractional-order controllers because they are less susceptible to oscillations and measurement noise. For a DC-microgrid with multiple random sources and strong demand for DC, the new controller is presented in Figure 1.

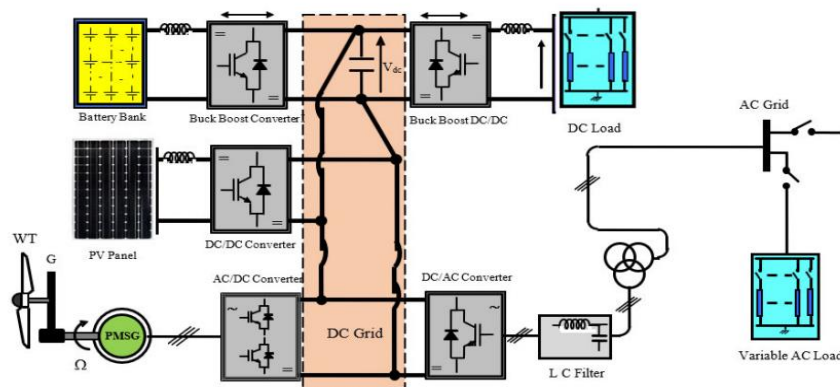


Fig 1. Hybrid system structure

This may be done using low-level controllers like energy management units (EMU) and intelligent Fractional-Order PIDs (IFO-PIDs). By enhancing SSCs, the author hopes to increase the amount of electricity provided by RES like solar PV and wind (source-side converters). The energy management unit adjusts DC-link voltage and reactive power to their reference values in the second phase of DC-microgrid quality improvement (EMU). Because of its important contribution to the area, this work stands out among the others. For a DC microgrid with many stochastic sources and huge DC demands, a new fractional order PID (FO-PID) controller and fuzzy logic method have been developed. This approach seeks to minimize the FO sensitivity of the PID to external disturbances by using a fuzzy gain supervisor based on fuzzy logic. Reducing the strategy's sensitivity to parameter fluctuation and increasing resilience and global stability are the goals of this method.

II. EXISTING SYSTEM

An integrated smart DC-microgrid topology displays a hybrid energy system with wind, solar, and BSS energy sources all associated to the DC-link via their own converters, which is what the existing topology depicts. Among the most important loads in a smart university's laboratories are benches, fans, and lights. The MPPT approach is used in both wind and solar conversion systems. Control modes are selected based on a calculation

of how much energy is consumed and produced. As a result, Fig. 2 depicts the general energy management controller structure.

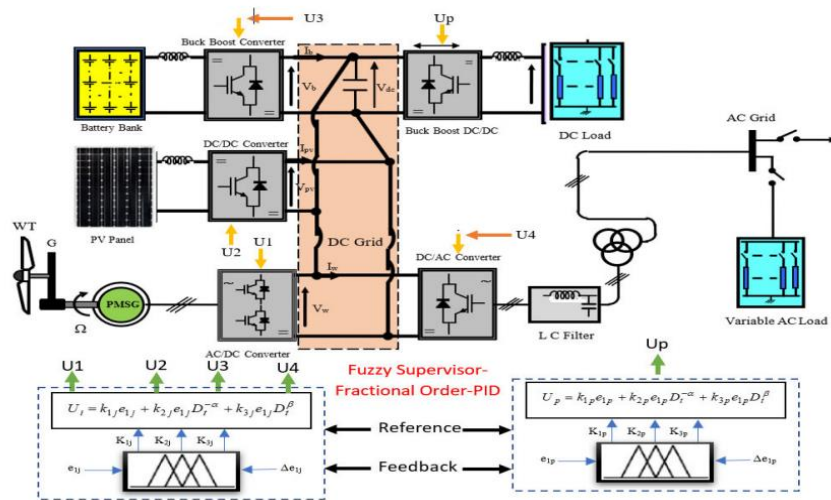


Fig.2 Existing system with Fuzzy-FOPID controller

III. PROPOSED SYSTEM

With the proposed system, a smart DC-microgrid is linked with a hybrid energy system, which includes wind, solar, and the BSS, all of which are associated to the DC-link capacitor via their particular converters. FOPID is used to control the converters on the source side. For example, in a smart university, fans, laboratory experimental benches, and lighting may be considered high priority loads. The suggested ANFIS approach regulates the AC/DC converters on the load side. On both wind and solar (PV) systems, algorithms for tracking the maximum power point are employed to ensure that they operate at full capacity. The energy management system calculates the overall quantity of energy used and generated in order to pick the most effective control strategies. The recommended set-up as indicated in Figure.3.

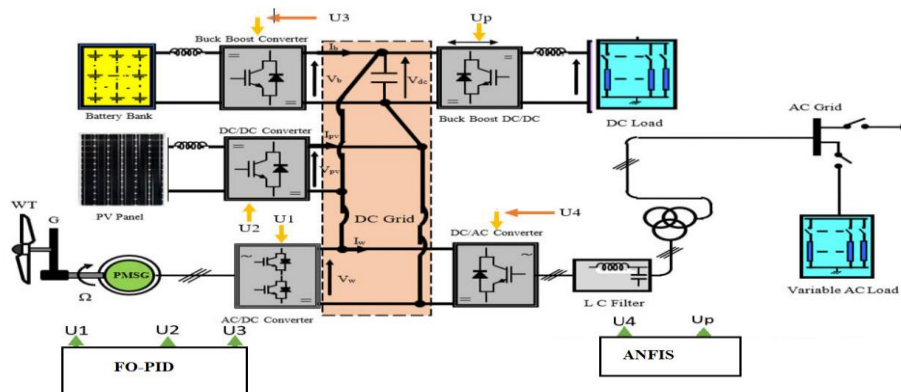


Fig.3 Proposed system with ANFIS controller Structure.

IV. MATHEMETICAL MODELLING

MODELLING OF WIND SYSTEM

Calculating how wind power is converted into useful energy may be done using the following formula:
Calculating how wind power is converted into useful energy may be done using the following formula

$$P_m = \frac{1}{2} \rho C_p(\beta, \lambda) A v^3 \quad (1)$$

$$T_m = \frac{P_m}{\omega_t} \quad (2)$$

$$C_p(\beta, \lambda) = \frac{1}{2} \left(\frac{116}{\lambda_i} - 0.4\beta - 5 \right) e^{-\left(\frac{21}{\lambda_i}\right)} \quad (3)$$

$$\lambda_i^{-1} = (\lambda + 0.88\beta)^{-1} - 0.0365(1 + \beta^3)^{-1} \quad (4)$$

$$\lambda = \frac{\omega_t R}{v}, \quad (5)$$

where, v is speed of the wind, t is speed of the turbine, β is the pitch angle, R is blades radius, C_p is coefficient of the power, and A is the area of the blade. Permanent (PSMG) Magnet Synchronous Generator is used to convert the wind energy into electricity,

$$v_{dq} = R_{dq} i_{dq} + L_{dq} \dot{i}_{dq} + \psi_{dq} \omega_m \quad (6)$$

$$J \dot{\omega}_m = T_m - T_e - f f v \omega_m \quad (7)$$

$$T_e = \frac{2}{3} p \psi_{dq}^T i_{dq} \quad (8)$$

where, $i_{dq} = \begin{bmatrix} i_d \\ i_q \end{bmatrix}$ T signifies the torque, and f represent the viscous friction coefficient., $L_{dq} = \begin{bmatrix} L_d & 0 \\ 0 & L_q \end{bmatrix}$ J is the inertia for the dq inductances matrix., $\psi_{dq} = \begin{bmatrix} \psi_f \\ 0 \end{bmatrix}$ the voltage stator vector is represented by this equation: $v_{dq} = \begin{bmatrix} v_d \\ v_q \end{bmatrix}$ $R_{dq} = \begin{bmatrix} R_d & 0 \\ 0 & R_q \end{bmatrix}$ resistor matrix for the stator. The SSCs model expressed before the proposed control mechanism can be designed. As a result, the wind source converter model (see Figure 3.1) is exposed as

$$\frac{dV_\omega}{dt} = \frac{I_\omega}{C_\omega} - \frac{I_{L\omega}}{C_\omega} \quad (9)$$

$$\frac{V_\omega}{L_\omega} = \frac{dI_\omega}{dt} + (1-U_1) \frac{V_{dc}}{L_\omega} - D_1 \quad (10)$$

$$\frac{dV_{dc}}{dt} = (1-U_1) \frac{I_{L\omega}}{C_{dc}} - \frac{I_{O\omega}}{C_{dc}} + D_2 \quad (11)$$

I_ω stands for inversely-rectified wind current, L_ω stands for inverse-rectified inductance, $I_{L\omega}$ stands for inversely-rectified inductor current, V_ω stands for inversely-rectified input voltage, U_1 , V_{dc} , and D_1 and D_2 stand for dynamical uncertainty in energy stage parameters.

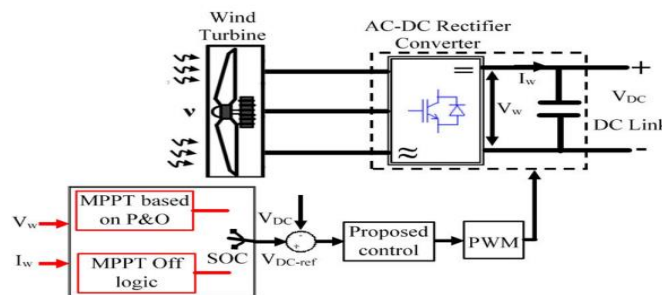


Fig 4. Control system with Wind energy system.

An energy management unit (EMU) is proposed in order to lesser generated power and maintains a stable power in stand-alone system if there is an abundance of energy and no battery storage capacity, as outlined in the article. This is how off-voltage MPPT's reference is set up:

$$V_{ref} = \frac{P_L - P_w}{I_w} \quad (12)$$

where, Load power and wind energy system power are both referred to as P_L and P_w , respectively.

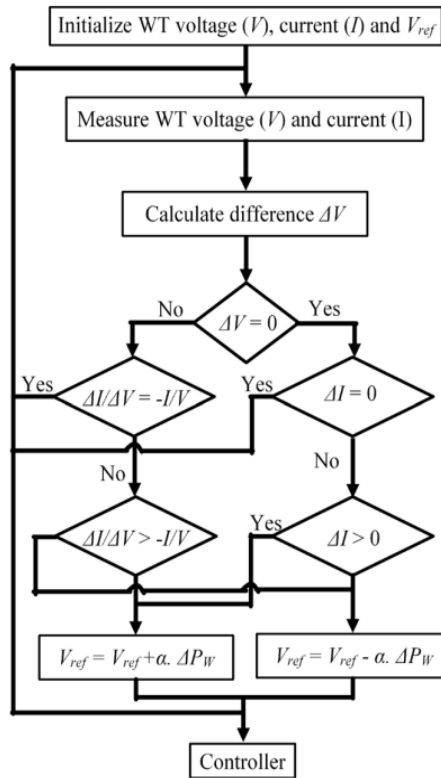


Fig.5 Flow chart of MPPT algorithm for wind system.

MODELLING OF SOLAR POWER SYSTEM

As a part of the solar conversion system (SCS), a DC-DC boost converter is used to connect a PV panel to a DC-link. The following is a mathematical representation of the SCS:

$$\frac{dV_{pv}}{dt} = \frac{I_{pv}}{C_{pv}} - \frac{I_{Lpv}}{C_{pv}} \quad (13)$$

$$\frac{V_{pv}}{L_{pv}} = \frac{dI_{pv}}{dt} + (1 - U_2) \frac{V_{dc}}{L_{pv}} - D_3 \quad (15)$$

$$\frac{dV_{dc}}{dt} = (1 - U_2) \frac{I_{Lpv}}{C_{dc}} - \frac{I_{Opv}}{C_{dc}} + D_4 \quad (16)$$

Figure .5 shows the dynamical uncertainty in the energy stage parameters, D3 and D4, which are shown as a function of the PV current, inductance, voltage, and LLpv (the inductor current) as well as the control signal U2.

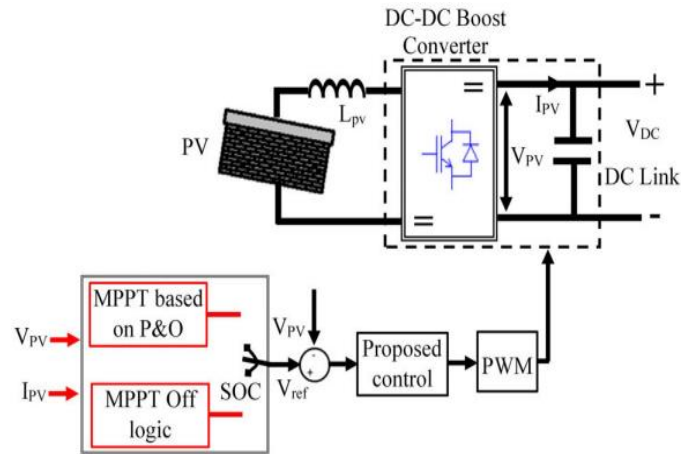


Fig.6 Solar energy system with controller.

For example, in the case of excessive power generation and no battery storage capacity, the recommended energy management system's PV controller is shifted from MPPT mode to off-MPPT mode in order to maintain a balanced power supply in a stand-alone system, as seen in Figs. 6 and 7. In off-MPPT, it serves as a point of reference.

$$V_{ref} = \frac{P_L - P_{pv}}{I_{pv}} \quad (17)$$

where, P_L is power at the Load and P_{pv} is wind energy system power.

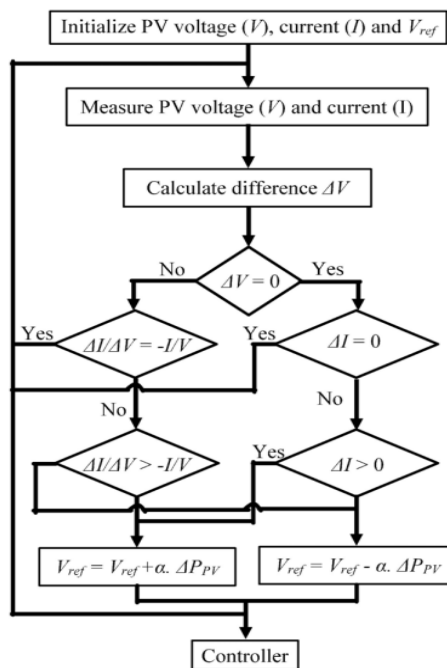


Fig 7. Flow chart of MPPT algorithm for solar power generation.

MODELLING OF BATTERY SYSTEM

An ordinary battery is associated to the microgrid's DC link via a DC-DC bidirectional buck-boost converter in this application (see Figure 8). In order to keep the DC-link voltage stable, this converter is needed. Fig. 8 illustrates the recommended technique for designing a voltage controller based on the DC-link voltage and battery reference current.

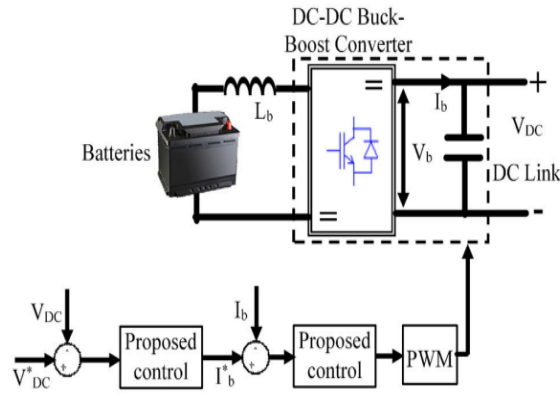


Fig 8 Controller with Battery storage system .

The *SOC* of Battery model is demonstrated as defined below,

$$SOC = 100 \left(1 + \frac{\int I_{batt} dt}{Q} \right) \quad (18)$$

The *SOC*, Controlling the quantity of electricity stored when charging is a crucial aspect. The suggested supervisory system must detect the battery *SOC* so that it can make decisions based on its current status and the amount of power it requires. The *SOC* limitations influence the battery's energy constraints:

$$SOC_{min} \leq SOC \leq SOC_{max} \quad (19)$$

where, SOC_{max} and SOC_{min} are maximum and minimum acceptable states for the battery safety. The BSS converter model is assumed as:

$$\frac{V_b}{L_b} = \frac{dI_{Lb}}{dt} + U_3 \frac{V_{dc}}{L_p} - D_5 \quad (20)$$

$$\frac{dV_{dc}}{dt} = U_3 \frac{I_b}{C_{dc}} + \frac{I_{ob}}{C_{dc}} - D_6 \quad (21)$$

where, I_b signifies the battery current , V_b signifies the battery voltage , U_3 signifies the controller signal, D_5 and D_6 represents dynamics uncertainty in the energy stage parameters.

AC GRID MODEL

A buck-to-buck converter is used in wind and AC grid conversions (see Figure. 9).

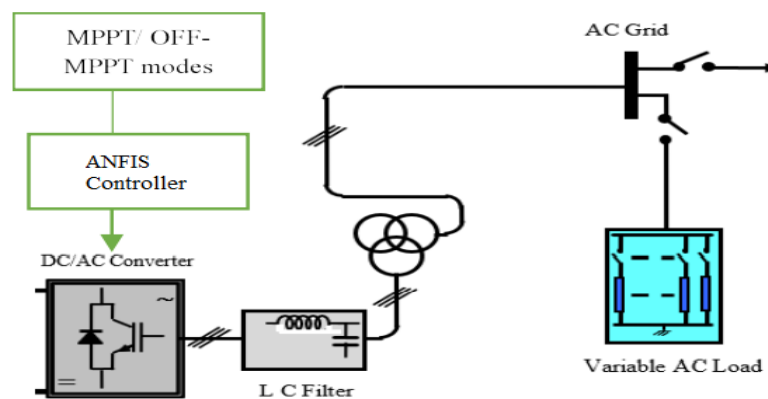


Figure 9. AC load system.

To express the AC grid converter mathematical model, we can use the following notation:

$$\frac{dV_g}{dt} = \frac{I_g}{C_g} - \frac{I_{Lg}}{C_g} \quad (22)$$

$$\frac{V_g}{L_g} = \frac{dI_g}{dt} + (1 - U_4) \frac{V_{dc}}{L_g} - D_7 \quad (23)$$

$$\frac{dV_{dc}}{dt} = (1 - U_4) \frac{I_{Lg}}{C_{dc}} + \frac{I_{og}}{C_{dc}} + D_8 \quad (24)$$

where, I_g represents the grid rectified current, V_g represents grid input rectified voltage, U_4 represents the controller signal, D_7 and D_8 represents the energy stage parameters dynamics uncertainty, I_{Lg} represents the inductor current, and C_{dc} represents the DC-link capacitor.

The following is a deductive proof of a generalized compact form:

$$\frac{dV_j}{dt} = \frac{I_j}{C_j} - \frac{I_{Lj}}{C_j} \quad (25)$$

$$\frac{V_j}{L_j} = \frac{dI_j}{dt} + (1 - U_i) \frac{V_{dc}}{L_j} - D_i \quad (26)$$

$$\frac{dV_{dc}}{dt} = (1 - U_i) \frac{I_{Lj}}{C_{dc}} + \frac{I_{oj}}{C_{dc}} + D_{i+1} \quad (27)$$

where, the subscript j indicates the given sub-terms of the supplied converters (w,pv,bn and g). The subscript i denotes two in the case of PV, one in the case of wind, three in the case of Battery, and four in the case of AC grid.

LOAD SIDE CONVERTERS (LSCs) MODEL

There are several parallel converters that can be mathematically modelled as follows:

$$\frac{U_p V_{dc}}{L_b} = \frac{dI_{Lb}}{dt} + \frac{V_{loadp}}{L_p} - DI_{LP} \quad (28)$$

$$\frac{dV_{Loadp}}{dt} = \frac{I_{LP}}{C_p} + \frac{V_{loadp}}{R_{LP} C_c} - DV_{Loadp} \quad (29)$$

where, U_p represents the control law, I_{LP} represents the inductor current, V_{loadp} represents the voltage at the load, DV_{Loadp} represents the voltage dynamics uncertainty, and DI_{LP} represents the current dynamics uncertainty

V. PROPOSED ANFIS CONTROLLER

The ANFIS makes use of neural networks and fuzzy logic, as well as lower-level computing abilities. In order to simulate complex and nonlinear systems, ANFIS requires just a few simple input and output parameters. The fuzzy interference system may be fine-tuned with the help of a neural network. In order to build correlations between input and output, ANFIS' hybrid learning technique makes use of both human experience and data on input and output. Analyze non-linear functions and detect non-linear parameters in online control using ANFIS, and use time series models to forecast parameters in time series models the layered structure of the ANFIS, as shown in Figure 10, is typical of the system. Nodes for input, fuzzification and product, normalization and defuzzification are included in this system. Squares indicate adaptive nodes, while circles represent fixed nodes. $P_G(t)$ and $P_L(t)$ are the inputs of ANFIS, and our output target is a reference power for HRES (P) based on $P_G(t)$. The new ANFIS approach is able to produce and alter rules quickly because of the use of relative parameters.

This is the initial step in the process, and it should be taken first. For the Takagi-Sugeno interference system, the two fuzzy layers are governed by the same rule set. (30) and Eq. (31)

$$\begin{aligned} &\text{Rule 1: If } P_G(t-1) \text{ is } C_1 \text{ and } P_L(t) \text{ is } D_1 \text{ then} \\ &f_1 = m_1 P_G(t-1) + n_1 P_L(t) + k_1 \end{aligned} \quad (30)$$

$$\begin{aligned} &\text{Rule 2: If } P_G(t-1) \text{ is } C_2 \text{ and } P_L(t) \text{ is } D_2 \text{ then} \\ &f_2 = m_2 P_G(t-1) + n_2 P_L(t) + k_2 \end{aligned} \quad (31)$$

where, the linear parameters are represented by m_1, m_2, n_1, n_2, k_1 and k_2 , whereas the non-linear parameters are represented by C_1, C_2, d_1 and d_2 . Figure.11 depicts the ANFIS's fuse reasoning. To determine activation levels related to fuzzy rules, one can use W-Xi (a)-Y I (b) as a relation, where the logical operator "and" can be optimized by using a permanent t-norm. Eq. provides the outcome of each rule as a linear mix of the parameters of each rule's antecedents (32)

$$f_i = m_i P_G(t-1) + n_i P_L(t) + k_i, i = 1, 2, \dots \quad (32)$$

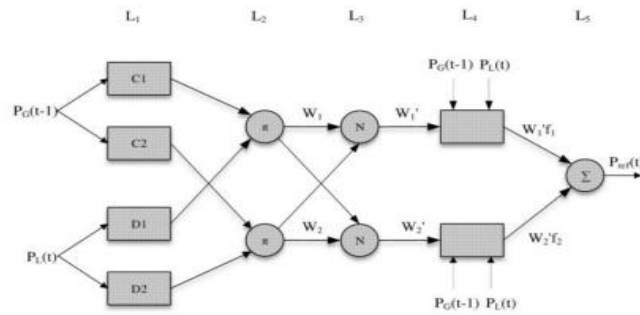


Fig.10. Structure of the ANFIS

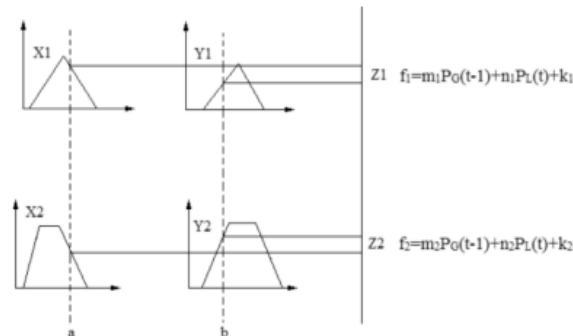


Fig.11 First order Takagi-sugeno fuse reasoning

Rule activation degrees are multiplied by the individual rule outputs provided in Eq. f, and the result is the output of the model f. (33)

$$f = \frac{\sum W_i' f_i}{\sum W_i}, i = 1, 2, \dots \quad (33)$$

where, W_i indicates the normalized value, which comprises the sum of W_1 and W_2 . The ANFIS layer structure is elegantly shown in Fig. 4.4 and the corresponding depiction is supplied as follows

Layer 1: Fuzzification is the name given to this layer. This layer calculates the number of degrees of membership functions for each input variable. The error (e) and the error change (\dot{e}) are used as the ANFIS input variables. Reduced error is achieved by using trapezoidal and triangular enrollment capacity, with the following node conditions:

$$O_i^1 = \mu_{A_i}(x) = \frac{1}{1 + \left[\frac{(x - c_i)}{a_i} \right]^{2b_i}} \quad (34)$$

Assuming that the input to the node function is x , A_i and the membership function is μ_{A_i} , the premise parameter set is as follows:

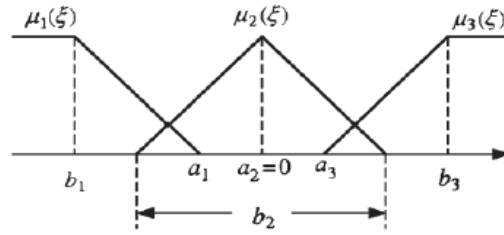


Fig.12 Fuzzy membership functions.

Layer 2: It's a layer that does rule inference. In this layer, all of the nodes are fixed nodes that multiply incoming signals and send the resulting signal out. Node outputs represent the firing strength of a fuzzy rule for a given rule set.

$$O_i^2 = \mu_i = \mu(x)\mu(y) \quad i = 1, 2, 3 \quad (35)$$

Layer 3: This layer serves as a sort of baseline. In this layer, each circle node is labelled with the letter N. This node calculates the ratio of the rule's firing strength to the total firing strength of all rules.

$$O_i^3 = \bar{\mu}_i = \frac{\mu_i}{\mu_1 + \mu_2 + \mu_3} \quad i = 1, 2, 3 \quad (36)$$

Layer 4: The following layer is this one. There is an adaptive mode for all nodes.

$$O_i^4 = \bar{\mu}_i \cdot f_i = \bar{\mu}_i (a_0^i + a_1^i \epsilon) \quad i = 1, 2, 3 \quad (37)$$

where w_i is the Layer 3 output and (a_0, a_1) is the consequent parameter set.

Layer 5: The output layer is located on the current layer stack. To sum up all of the incoming signals in this layer, there is only one node marked that computes the overall output.

$$O_i^5 = \mu_i = \sum_i \bar{\mu}_i f_i \quad i = 1, 2, 3 \quad (38)$$

The back propagation error term is used to update all ANFIS parameters

$$\frac{\partial E}{\partial O^5} = k_1 \cdot e + k_2 \cdot \Delta e \quad (39)$$

The input signals error (e) and the change of error (Δe) multiplied by the coefficients k_1 and k_2 .

$$\alpha_{k+1} = \alpha_k - \eta \frac{\partial E}{\partial \alpha_k} \quad (40)$$

where α is any of the parameters of ANFIS and η is learning rate. The error will be reduced next training iteration.

VI.SIMULATION RESULTS

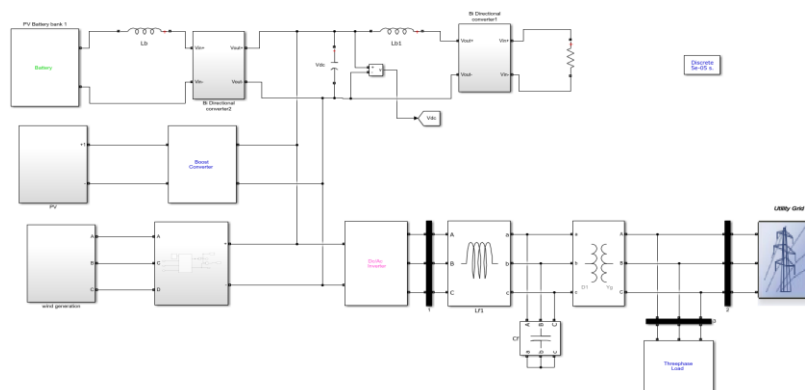


Fig.13 MATLAB/SIMULINK circuit diagram of the system

a) EXISITNG RESULTS

Case1: Under step changes speed

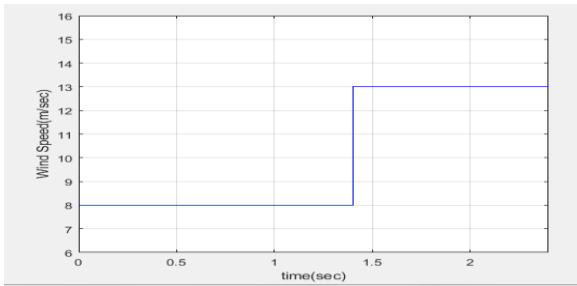


Fig.14 Speed of the wind

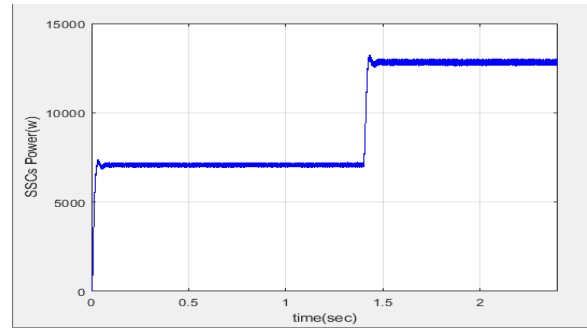


Fig.18 SSCs power

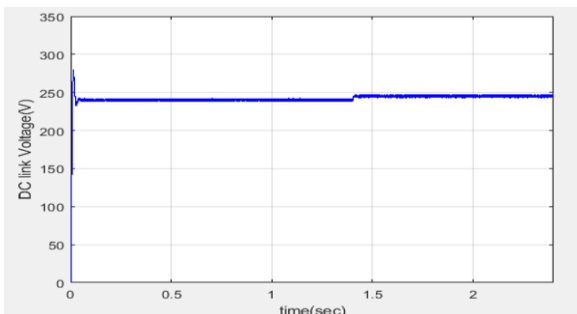


Fig.15 Power of the wind

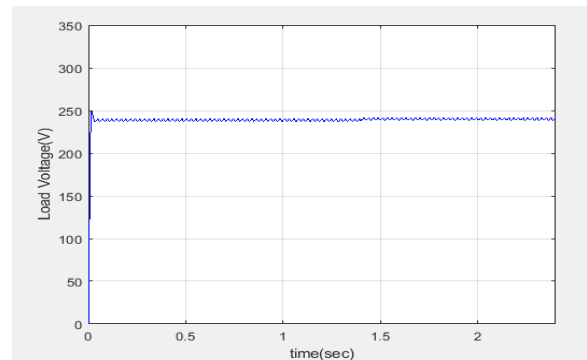


Fig.19 Load Voltage

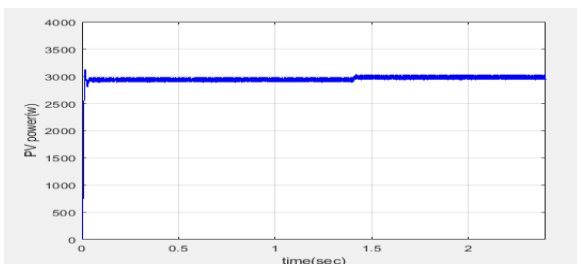


Fig.16 Solar power.

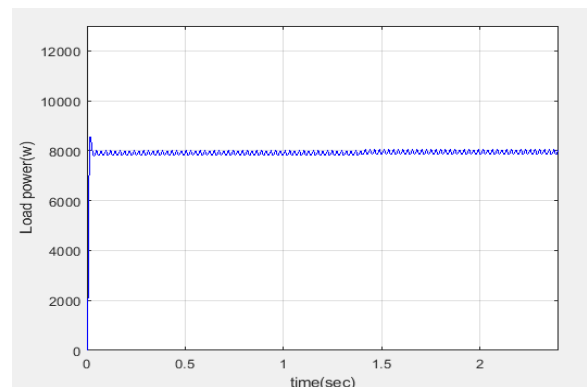


Fig.20 Load power

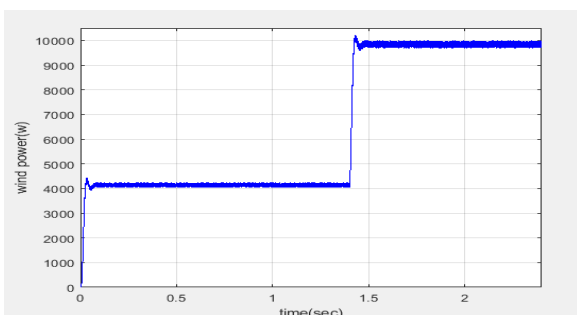


Fig.17 Wind power

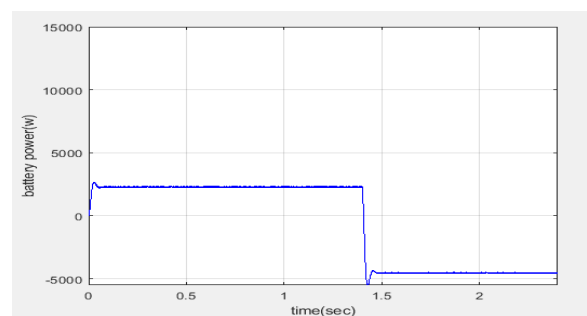


Fig.21 Battery power

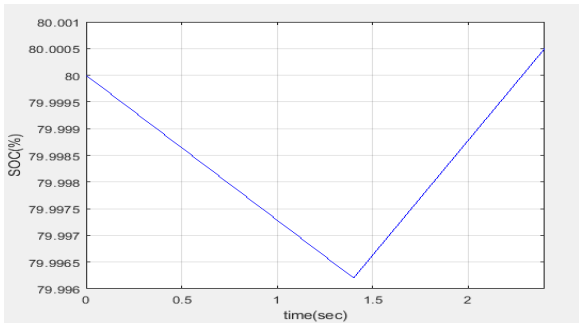


Fig .22 Battery SOC%

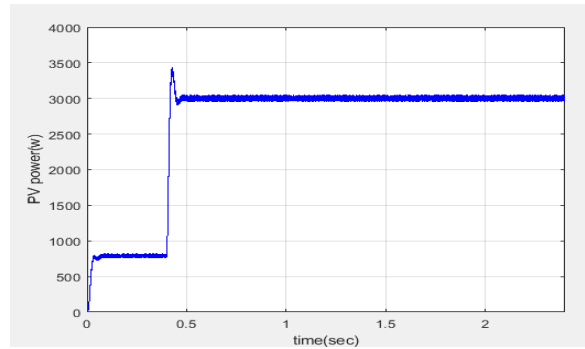


Fig.26 PV power

Case2: Under random speed

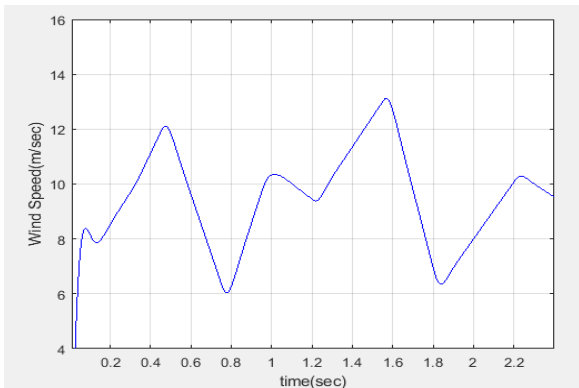


Fig .23 Random wind speed.

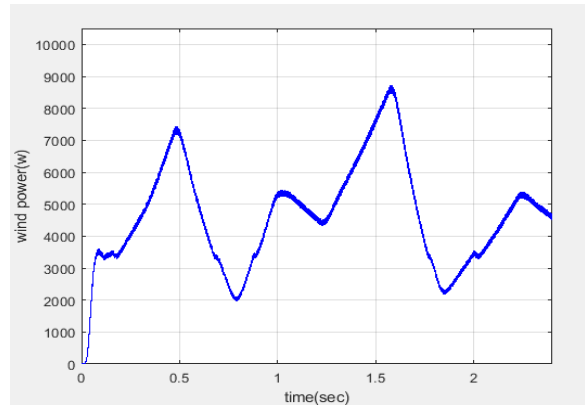


Fig .27 Wind power

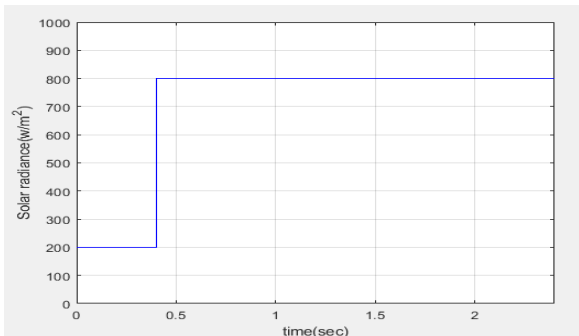


Fig .24 Solar radiance.

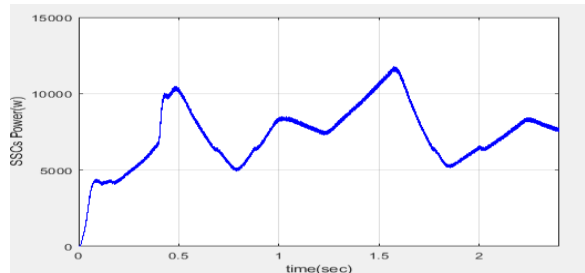


Fig.28 Solar power

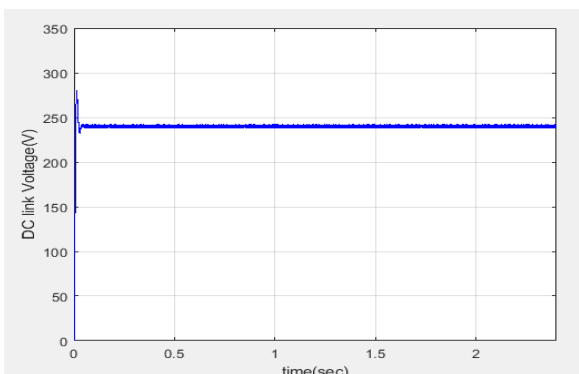


Fig .25 DC-link voltage under random variation

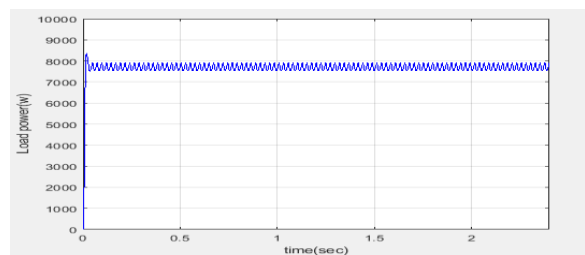


Fig.29 Load power

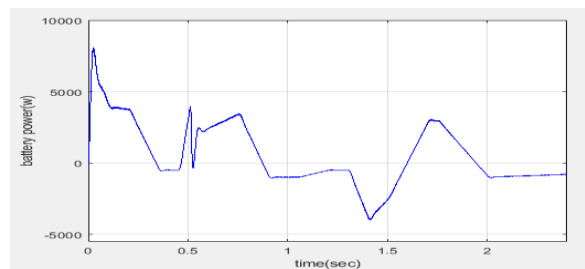


Fig.30 Battery power

b) EXTENSION RESULTS

Case1: Under step changes speed

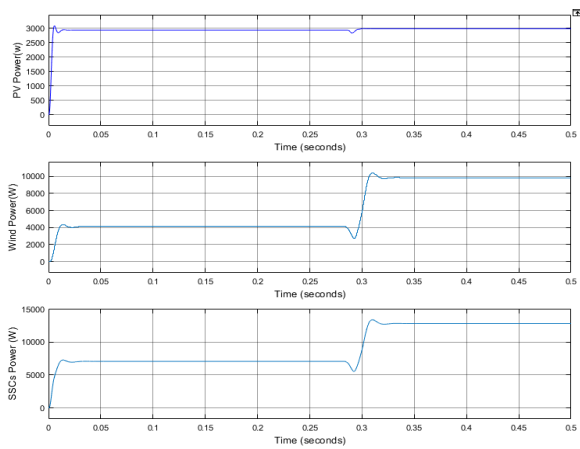


Fig.31 PV, Wind and SSCs power

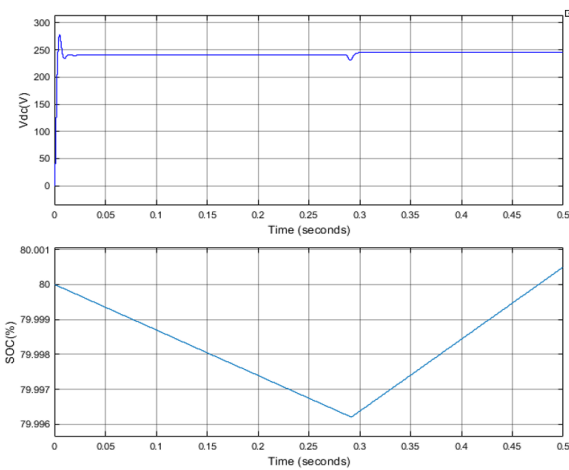


Fig.32 DC link voltage and SOC%

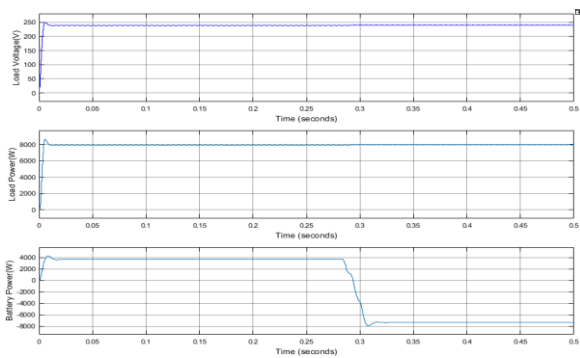
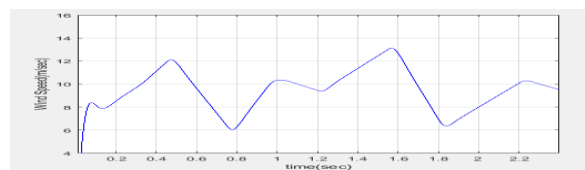


Fig .33 Load voltage, Load power and Battery power

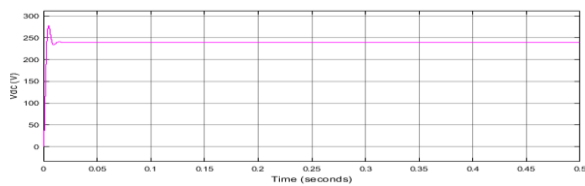
Case2: Under random speed



(a)



(b)



(c)

Fig.34 (a)Wind speed (b)Solar irradiance (c) DC link voltage

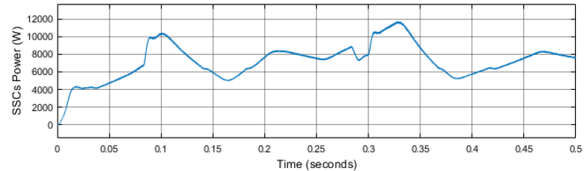
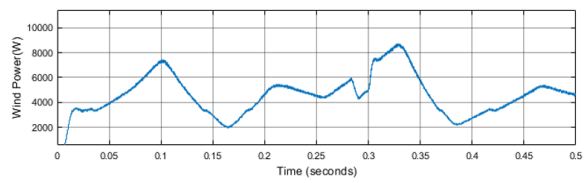
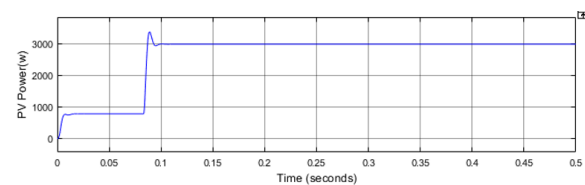


Fig.35 PV, Wind and SSCs power

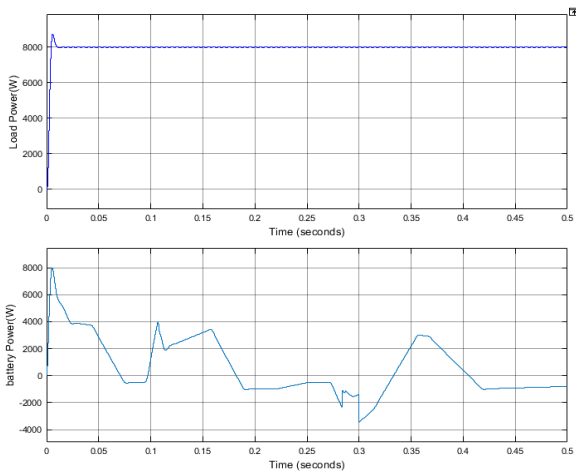


Fig.36 Load and Battery power

CONCLUSION

Hybrid energy sources associated to a smart grid via DC-link voltage can be controlled using an ANFIS controller, which is proposed in this work. The DC-hybrid microgrid's energy source includes batteries, wind power, and solar power. The DC-DC-microgrid microgrid's novel intelligent FO-PID approach allows it to gather the maximum amount of power from RESs (wind and PV). The most cost-effective energy sources to use when constructing a microgrid are (Wind and PV). In order to regulate the load converters, we employ the ANFIS control technique. Stable output power and uninterrupted service are provided by the ANFIS controller proposed in this paper. The proposed simulation results are implemented in the MATLAB/Simulink environment.

REFERENCES

- [1] H. T. Dinh et.al., “A home energy management system with renewable energy and energy storage utilizing main grid and electricity selling,” *IEEE Access*, vol. 8, pp. 49436–49450, 2020.
- [2] C. Byers et.al., “Additional capacity value from synergy of variable renewable energy and energy storage,” *IEEE Trans. Sustain. Energy*, vol. 11, no. 2, pp. 1106–1109, Apr. 2020.
- [3] M. Rizwan et.al., “Hybrid Harris Hawks optimizer for integration of renewable energy sources considering stochastic behavior of energy sources,” *Int. Trans. Elect. Energy Syst.*, vol. 31, no. 2, 2021, Art. no. e12694, doi: 10.1002/2050-7038.12694.
- [4] Y. Sun et.al., “Overview of energy storage in renewable energy power fluctuation mitigation,” *CSEE J. Power Energy Syst.*, vol. 6, no. 1, pp. 160–173, 2020.
- [5] T. Salameh et.al., “Integrated standalone hybrid solar PV, fuel cell and diesel generator power system for battery or supercapacitor storage systems in khorfakkan, united arab emirates,” *Int. J. Hydrogen Energy*, vol. 46, no. 8, pp. 6014–6027, Jan. 2021.
- [6] M. Çolak et.al., “multi-criteria evaluation of energy storage technologies based on hesitant fuzzy information: A case study for turkey,” *J. Energy Storage*, vol. 28, Apr. 2020, Art. no. 101211.
- [7] M. A. Hannan et.al., “Review of energy storage systems for electric vehicle applications: Issues and challenges,” *Renew. Sustain. Energy Rev.*, vol. 69, pp. 771–789, Mar. 2017.
- [8] R. Amirante et.al., “Overview on recent developments in energy storage: Mechanical, electrochemical and hydrogen technologies,” *Energy Convers. Manage.*, vol. 132, pp. 372–387, Jan. 2017.
- [9] T. Ma et.al., “Development of hybrid battery–supercapacitor energy storage for remote area renewable energy systems,” *Appl. Energy*, vol. 153, pp. 56–62, Sep. 2015.
- [10] X. Wang et.al., “A novel controller of a battery-supercapacitor hybrid energy storage system for domestic applications,” *Energy Buildings*, vol. 141, pp. 167–174, Apr. 2017.
- [11] A. Kadri et.al., “Energy management and control strategy for a DFIG wind turbine/fuel cell hybrid system with super capacitor storage system,” *Energy*, vol. 192, Feb. 2020, Art. no. 116518.
- [12] A. K. Barik et.al., “Optimal voltage–frequency regulation in distributed sustainable energy based hybrid microgrids with integrated resource planning,” *Energies*, vol. 14, no. 10, p. 2735, May 2021, doi: 10.3390/en14102735.
- [13] A. K. Barik et.al., “Recent trends and development in hybrid microgrid: A review on energy resource planning and control,” *Int. J. Sustain. Energy*, vol. 4, pp. 1–15, Apr. 2021, doi: 10.1080/14786451.2021.1910698.
- [14] H. Kakigano et.al., “Distribution voltage control for DC microgrids using fuzzy control and gain-scheduling technique,” *IEEE Trans. Power Electron.*, vol. 28, no. 5, pp. 2246–2258, May 2013.
- [15] D. A. Aviles et.al., “An energy management system design using fuzzy logic control: Smoothing the grid power profile of a residential electro-thermal microgrid,” *IEEE Access*, vol. 9, pp. 25172–25188, 2021.
- [16] M. Kumar et.al., “Control strategies of a DC microgrid for grid connected and islanded operations,” *IEEE Trans. Smart Grid*, vol. 6, no. 4, pp. 1588–1601, Jul. 2015.
- [17] H. Hajebrahimim et.al., “A new energy management control method for energy storage systems in microgrids,” *IEEE Trans. Power Electron.*, vol. 35, no. 11, pp. 11612–11624, Mar. 2020.
- [18] Y. Xu et.al., “Optimal control based energy management of multiple energy storage systems in a microgrid,” *IEEE Access*, vol. 6, pp. 32925–32934, 2018.
- [19] A.-R.-I. Mohamed et.al., “Seamless formation and robust control of distributed generation microgrids via direct voltage control and optimized dynamic power sharing,” *IEEE Trans. Power Electron.*, vol. 27, no. 3, pp. 1283–1294, Mar. 2012.
- [20] B. A. Martinez-Treviño et.al., A. Cid-Pastor, and L. Martinez-Salamero, “Sliding-mode control of a boost converter under constant power loading conditions,” *IET Power Electron.*, vol. 12, no. 3, pp. 521–529, 2019.